J|A|C|S COMMUNICATIONS

Published on Web 04/28/2010

Supramolecular n/p-Heterojunction Photosystems with Antiparallel Redox Gradients in Electron- and Hole-Transporting Pathways

Naomi Sakai,* Rajesh Bhosale, Daniel Emery, Jiri Mareda, and Stefan Matile*

Department of Organic Chemistry, University of Geneva, 1211 Geneva 4, Switzerland

Received March 8, 2010; E-mail: stefan.matile@unige.ch

The efficiency of organic optoelectronic devices depends on, among other things, their ability to generate charges and transport them to the electrodes.[1−13] In bilayer and bulk n/p-heterojunction (BHJ)[2−4] organic solar cells, electron (e^-)- and hole (h^+)-transporting materials are arranged in different ways for optimum charge transport, via highly ordered and conductive materials in the former and efficient charge separation at very large electron donor−acceptor interfaces in the latter. Supramolecular n/p-heterojunctions (SHJs),[1,5−10,12,13] in which e^-- and h^+-transporting channels are separated and aligned on the molecular level, have been proposed to combine these two advantages. Lessons from nature[1] further suggest that SHJs should be panchromatic (to capture all light) and funnel electrons and holes in opposite directions along oriented coaxial molecular e^- (or n)- and h^+ (or p)-transporting channels. However, the construction of antiparallel gradients in e^- and h^+ channels in SHJ photosystems has not been possible to date because of the formidable synthetic organic and supramolecular chemistry challenges involved, and their significance for function therefore remains unknown. Here we report the creation of the first SHJs with oriented multicolored antiparallel redox gradients (OMARG-SHJs)[1] and demonstrate that both gradients are needed to achieve photoinduced charge separation over very long distances.

Zipper assembly has recently been introduced for construction of ordered architectures with molecular-level precision on solid substrates. In zipper assembly, naphthalenediimide (NDI)[1] chromophores attached to *p*-oligophenyl (POP) or *p*-oligophenylethynyl (OPE) chromophores are assembled step-by-step to build mutually interdigitating π stacks along interdigitating rigid-rod scaffolds (Figures 1A and 2). Molecular dynamics (MD) simulations confirmed that intact intrastack hydrogen-bonded chains (Figure 1A) and interstack ion pairing and hydrophobic domains (Figure 2A) are perfectly placed to stabilize highly ordered π stacks along uniformly oriented rigid-rod scaffolds. Because their HOMO−LUMO gap decreases with increasing LUMO energy, NDIs are ideal for colorizing and building redox gradients into the e^--transporting π stacks (Figure 1B). OPE hole acceptors and POP donors should suffice for engineering a minimalist gradient into the h^+ channel (Figure 1B).

We designed Au−**1**−(**2**−**3**−)$_m$(**4**−**5**−)$_n$ architectures to function as OMARG-SHJ photosystems (Figure 1). If the ineffective N in **1** is ignored, this architecture contains antiparallel two-component R → Y and POP → OPE gradients in the e^-- and h^+-transporting pathways and is thus designated as a 2 + 2 OMARG-SHJ (Table 1). In this system, photoexcited R can transfer h^+ into proximal OPEs and e^- down the R → Y gradient toward the gold electrode, where h^+ cannot follow and recombine because of the POP−Y barrier. OPE excitation followed by e^- injection into R stacks gives the same.[12] Y can catch a photon and transfer h^+ to POP and down the POP → OPE gradient, where e^- is excluded because of the opposing R → Y gradient.

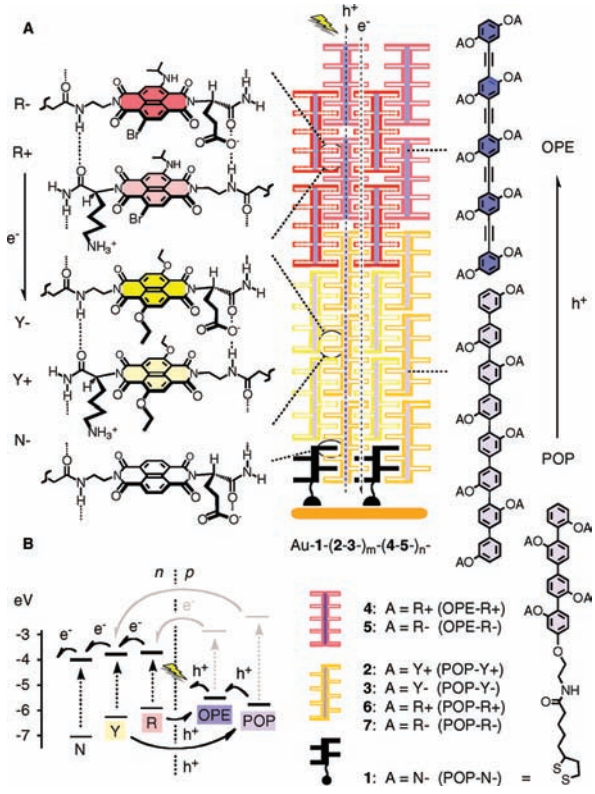

Figure 1. (A) Molecular structures and hypothetical OMARG-SHJ architecture Au−**1**−(**2**−**3**−)$_m$(**4**−**5**−)$_n$ of POP−N initiator (**1**) and POP−Y (**2**, **3**) and OPE−R (**4**, **5**) propagators on gold (for **8** and the full structures, see Figure 3 and the Supporting Information).[14] (B) HOMO and LUMO levels show photoinduced (dashed arrows) e^- (gray) and h^+ (black) injection into e^- (n)- and h^+ (p)-transporting pathways (bold).

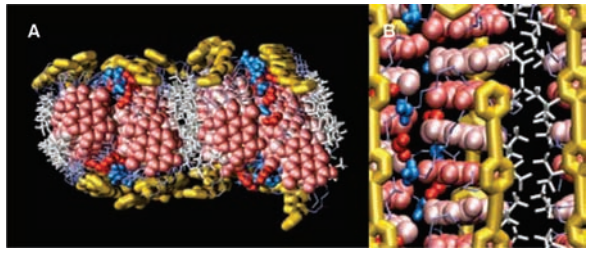

Figure 2. MD simulations of OPE−R zipper architectures −(**4**−**5**−)$_n$ in (A) top and (B) side views. Color key: R, garnet (light and dark for different molecules); OPE, gold; carboxylate anions, red; ammonium cations, blue; hydrophobic isopropyl domains, silver.

The building blocks **1**−**8** needed to assemble Au−**1**−(**2**−**3**−)$_m$(**4**−**5**−)$_n$ and the control systems have previously been synthesized and characterized in detail (Figure 3).[1,12−14] In brief, zipper architectures produce smoother surfaces and generate more

photocurrent than comparable architectures such as those produced by conventional layer-by-layer (LBL) assembly.[12,13] The occurrence of ultrafast R → OPE and Y → POP h^+ and OPE → R e^- transfer has been confirmed by transient absorption spectroscopy.[12,13] R → Y e^- and POP → OPE h^+ transfer is energetically favorable and supported by fluorescence quenching experiments in solution (Figure S6).[14] Transient absorption experiments with the functional OMARG-SHJs were not meaningful because gold substrates are not transparent and the absorptions of the relevant NDI radical anions overlap strongly.

Zipper assembly of 2 + 2 OMARG-SHJs was initiated by deposition of initiator **1** on gold electrodes following routine procedures.[1,14] The obtained Au−**1** monolayer was dipped into a solution of POP−Y propagator **2**. The lower Y's of **2** were expected to stack with the N's of **1**, whereas the upper Y's remain free as "sticky ends" to zip up with the anionic POP−Y **3**, which in turn can zip up with the cationic POP−Y **2**, and so on. To incorporate antiparallel redox gradients into the system, Au−**1**−(**2**−**3**−)$_4$**2**− was subjected to dip-wash cycles with anionic OPE−R **5** and cationic OPE−R **4**.

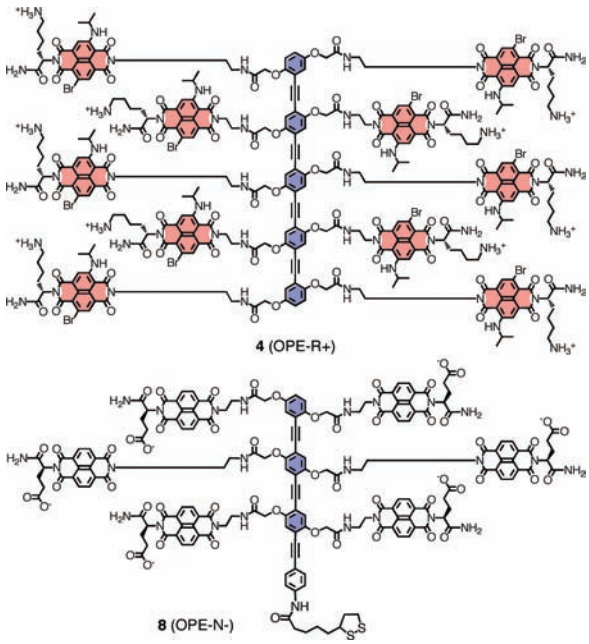

Figure 3. Selected monomer structures (compare with Figure 1).

The growth of OMARG-SHJs and the controls was monitored by photocurrent generation with triethanolamine (TEOA) as the electron donor (Figure 4A,C).[1,12−14] The mass deposited per layer under the same conditions was determined electromechanically with a quartz-crystal microbalance (QCM; Figure 4B,D).[1,12−14]

Absolute photocurrent values were irrelevant in the context of this study because intrinsic values in unicolor systems already differ substantially.[15,16] Most importantly, R zippers generate significantly more photocurrent than Y zippers.[12,13,15,16] These known intrinsic differences between R and Y zippers were reproduced during the assembly of the first domain of mixed zippers, where the R domains needed for controls (Figure 4A,C, ○) produced consistently more photocurrent than the Y domains needed for OMARG-SHJs (Figure 4A,C, ●). The complementary QCM data reproducibly confirmed that these difference originate chiefly from differences in the deposited mass (Figure 4B,D, open vs solid symbols).[15,16]

This situation changed dramatically with the addition of the second domain. For Au−**1**−(**2**−**3**−)$_m$**2**−(**5**−**4**−)$_n$, the change from POP−Y to OPE−R after deposition of 10 layers [L = 10; e.g., **1**−(**2**−**3**−)$_4$**2**] caused a steep increase in photocurrent generation (Figure 4A, ●, L = 10−15). This change reflected well the known differences between R and Y (Figure 4A, L = 1−10) and was thus unrelated to the OMARG−SHJs. Photocurrent densities reached saturation with roughly 40 layers, although small but steady increases could be noted until 50 layers and presumably more [critical thickness $L_C \geq 40$ (i.e., ∼80 nm);[17] Table 1, entry 1].

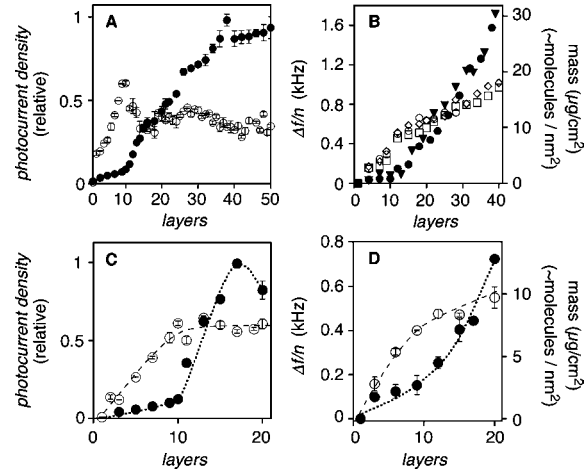

Figure 4. Photocurrent−layer (J−L) and QCM profiles of (A, B) OMARG- and anti-OMARG-SHJs and (C, D) single-gradient controls. (A, C) Changes in photocurrent density J as a function of the number of layers L for Au−**1**−(**2**−**3**−)$_4$**2**−(**5**−**4**−)$_n$ (A, ●), Au−**8**−(**4**−**5**−)$_4$**4**−(**3**−**2**−)$_n$ (A, ○), Au−**1**−(**2**−**3**−)$_4$**2**−(**7**−**6**−)$_n$ (C, ●), and Au−**1**−(**6**−**7**−)$_4$**6**−(**3**−**2**−)$_n$ (C, ○). (B, D) Changes in QCM frequencies $\Delta f/n$ as a function of L for the same systems. Trend curves were added in (C) and (D), and photocurrent densities were normalized to facilitate reading (A, J_{max} = 80 μA/cm^2; C, J_{max} = 123 μA/cm^2).[16,17] Error bars show standard errors of at least two independent experiments.

The complementary 2 + 2 anti-OMARG-SHJ Au−**8**−(**4**−**5**−)$_4$**4**−(**3**−**2**−)$_n$ contains antiparallel gradients that direct both e^- and h^+ in the wrong direction. This misconstruction produced a sharp decrease in photocurrent as soon as OPE−R layers were topped with POP−Y layers from L = 10 onward (Figure 4A, ○; Table 1, entry 4). The residual photocurrent, which was independent of assembly thickness up to L = 50, was of interest because it needs another photon to flow.[18]

Au−**1**−(**2**−**3**−)$_4$**2**−(**7**−**6**−)$_n$ was prepared as a formal 2 + 1 OMARG-SHJ photosystem, where the R → Y gradients in the e^- channel are preserved whereas the POP → OPE gradients in the h^+ channel are removed (Figure 4C, ●; Table 1, entry 5). As a result, the critical thickness dropped from $L_C \geq 40$ for the 2 + 2 OMARG-SHJs to L_C = 15 for the 2 + 1 OMARG-SHJs. This finding demonstrated that both POP → OPE and R → Y gradients in 2 + 2 OMARG-SHJs are essential for achieving photoinduced charge separation over long distances. Without a gradient in the h^+ channel, the hole can freely follow the electron moving down the coaxial gradient in the e^- channel and recombine.

In the 2 + 1 anti-OMARG configuration, the photocurrent did not decrease upon deposition of POP−Y layers (Figure 4C, ○). This was in agreement with unhindered photocurrent generation by POP−R, whereas POP−Y contributes less because e^- transfer from $Y^{-\bullet}$ to gold remains uphill.

Thickening the POP−Y domain (L_{D1}) in 2 + 2 OMARG-SHJs from 10 to 15 or 20 did not give the expected increase in the critical thickness, while the highest photocurrent observed at saturation identified the best L_{D1} to be 15 (Figure S2; Table 1, entries 2 and 3).

Table 1. Long-Distance Charge Separation in SHJ Photosystems[a]

entry	architecture[b]	designation[c]	m[d]	L_{D1}[e]	L_C[f]
1	Au−**1**−(**2**−**3**−)$_m$**2**−(**5**−**4**−)$_n$	2 + 2 OMARG	4	10	≥40
2	Au−**1**−(**2**−**3**−)$_m$(**4**−**5**−)$_n$	2 + 2 OMARG	7	15	≥40
3	Au−**1**−(**2**−**3**−)$_m$**2**−(**5**−**4**−)$_n$	2 + 2 OMARG	9	20	30
4	Au−**8**−(**4**−**5**−)$_m$**4**−(**3**−**2**−)$_n$	2 + 2 anti-OMARG	4	10	10
5	Au−**1**−(**2**−**3**−)$_m$**2**−(**7**−**6**−)$_n$	2 + 1 OMARG	4	10	15
6	Au−**1**−(**6**−**7**−)$_m$**6**−(**3**−**2**−)$_n$	2 + 1 anti-OMARG	4	10	10
7[g]	Au−**1**−(**2**−**3**−)$_n$	−	−	−	20
8[h]	Au−**8**−(**4**−**5**−)$_n$	−	−	−	20
9[h]	Au−**1**−(**6**−**7**−)$_n$	−	−	−	10

[a] Determined from photocurrent−layer (J−L) profiles (as in Figure 4).[14] [b] See Figure 1 for structures. [c] OMARG-SHJ, supramolecular n/p-heterojunction with oriented multicolor antiparallel redox gradients; i + j, number of components in the gradients in e^- and h^+ channels. [d] Number of bilayers in the first domain, excluding the initiator. [e] Total number of layers in the first domain, including the initiator (i.e., 2 + 2m in entries 1 and 3−6, 1 + 2m in entry 2). [f] Critical layer (corresponding to the critical thickness) where photocurrent saturation occurs. [g] Data from ref 13. [h] Data from ref 12.

Photocurrent saturation at the critical thickness L_C can occur because the surface architecture stops growing, because all of the light has been absorbed, or because charges start to recombine before reaching the electrodes. The QCM profiles demonstrated that neither hindered assembly nor disassembly account for the photocurrent saturation or decrease in OMARG-SHJs Au−**1**−(**2**−**3**−)$_4$**2**−(**5**−**4**−)$_n$ and all of the controls (Figure 4B,D).

The extent of charge recombination with increasing thickness of the system can serve as an indicator of the long-range supramolecular organization. Poor zipper architecture has been experimentally confirmed to account for the L_C value of 10 for POP−R zipper Au−**1**−(**6**−**7**−)$_n$ (Table 1, entry 9). The more impressive L_C value of 20 for POP−Y zipper Au−**1**−(**2**−**3**−)$_n$ and OPE−R zipper Au−**8**−(**4**−**5**−)$_n$ have been attributed to zipper architectures with high long-range order (Table 1, entries 7 and 8). The critical thickness $L_C \geq 40$ found for 2 + 2 OMARG-SHJ Au−**1**−(**2**−**3**−)$_m$**2**−(**5**−**4**−)$_n$ far exceeded those of simple SHJ zippers. The decreasing L_C found for $L_{D1} \geq 20$ could indicate the onset of exciton recombination in the expanded POP−Y domain (Table 1, entries 3 and 7). The constant $L_C \geq 40$ for various POP−Y domains with $L_{D1} < 20$ suggests that at this level, photocurrent saturation might originate from insufficient transmittance rather than exciton recombination. For architectures with 15 μg of R/cm^2 on one side of the electrode that according to AFM images[12,13] are homogenously smooth, the transmittance was calculated to drop below 35% (Figure S3). This suggested that long-distance photoinduced charge separation in OMARG-SHJ photosystems could approach infinity in the given detection system.

Acknowledgment. We thank R. S. K. Kishore, V. Ravikumar, A. Perez-Velasco, D.-H. Tran, L. Maffiolo, and S. Maity for contributions to the synthesis; P. Maroni and M. Borkovec for access to and assistance with the QCM; D. Jeannerat, A. Pinto, and S. Grass for NMR measurements; G. Hopfgartner, S. Michalet, P. Perrottet, and N. Oudry for MS; and the University of Geneva, the Swiss National Supercomputing Center (CSCS), and the Swiss NSF for financial support.

Supporting Information Available: Experimental details. This material is available free of charge via the Internet at http://pubs.acs.org.

References

(1) Bhosale, R.; Míšek, J.; Sakai, N.; Matile, S. *Chem. Soc. Rev.* **2010**, *39*, 138, and references therein.
(2) Thompson, B. C.; Fréchet, J. M. J. *Angew. Chem., Int. Ed.* **2008**, *47*, 58.
(3) Blom, P. W. M.; Mihailetchi, V. D.; Koster, L. J. A.; Markov, D. E. *Adv. Mater.* **2007**, *19*, 1551.
(4) Martín, N.; Sánchez, L.; Ángeles Herranz, M.; Illescas, B.; Guldi, D. M. *Acc. Chem. Res.* **2007**, *40*, 1015.
(5) Würthner, F.; Chen, Z.; Hoeben, F. J. M.; Osswald, P.; You, C.-C.; Jonkheijm, P.; Herrikhuyzen, J.; Schenning, A. P. H. J.; van der Schoot, P. P. A. M.; Meijer, E. W.; Beckers, E. H. A.; Meskers, S. C. J.; Janssen, R. A. J. *J. Am. Chem. Soc.* **2004**, *126*, 10611.
(6) Yamamoto, Y.; Zhang, G.; Jin, W.; Fukushima, T.; Ishii, N.; Saeki, A.; Seki, S.; Tagawa, S.; Minari, T.; Tsukagoshi, K.; Aida, T. *Proc. Natl. Acad. Sci. U.S.A.* **2009**, *106*, 21051.
(7) Kira, A.; Umeyama, T.; Matano, Y.; Yoshida, K.; Isoda, S.; Park, J. K.; Kim, D.; Imahori, H. *J. Am. Chem. Soc.* **2009**, *131*, 3198.
(8) Wasielewski, M. R. *Acc. Chem. Res.* **2009**, *42*, 1910.
(9) Snaith, H. J.; Whiting, G. L.; Sun, B.; Greenham, N. C.; Huck, W. T. S.; Friend, R. H. *Nano Lett.* **2005**, *5*, 1653.
(10) Yang, F.; Shtein, M.; Forrest, S. *Nat. Mater.* **2005**, *4*, 37.
(11) Morisue, M.; Yamatsu, S.; Haruta, N.; Kobuke, Y. *Chem.—Eur. J.* **2005**, *11*, 5563.
(12) Bhosale, R.; Perez-Velasco, A.; Ravikumar, V.; Kishore, R. S. K.; Kel, O.; Gomez-Casado, A.; Jonkheijm, P.; Huskens, J.; Maroni, P.; Borkovec, M.; Sawada, T.; Vauthey, E.; Sakai, N.; Matile, S. *Angew. Chem., Int. Ed.* **2009**, *48*, 6461.
(13) Kishore, R. S. K.; Kel, O.; Banerji, N.; Emery, D.; Bollot, G.; Mareda, J.; Gomez-Casado, A.; Jonkheijm, P.; Huskens, J.; Maroni, P.; Borkovec, M.; Vauthey, E.; Sakai, N.; Matile, S. *J. Am. Chem. Soc.* **2009**, *131*, 11106.
(14) See the Supporting Information.
(15) The higher photocurrents and greater mass deposited with R zippers than Y zippers can be explained by incomplete layer formation with POP−Y (or, less likely, overzipping with R). The slower assembly kinetics according to photocurrent generation with Y zippers (2 days) in comparison with R zippers (<1 day) and LBL controls[12,13] as well as the smooth surfaces in all zippers[12,13] imply the occurrence of extensive self-repair of incomplete layers with continuing assembly. The number of permanent errors in zipper architectures should differ for different monomer structures. Vigorous functional controls (capping, LBL), smooth surfaces, and high (in comparison with relevant controls) fill factors, photocurrents, critical thickness, etc., imply that the overall error frequency was low.
(16) *Absolute* photocurrent densities were not maximized, as they were not the main concern of this study. Elimination of surface plasmon resonance (SPR) quenching (using surfaces other than gold)[12,13] and total oxygen exclusion (glovebox level), among other things, would be expected to boost the photocurrent. The reproducibility in experiments with identical materials was excellent (Figure 4), and the batch-to-batch reproducibility was reasonable.
(17) The film thickness could be estimated assuming ~2 nm per layer, which is in accordance with the proposed suprastructure (Figure 1) and preliminary ellipsometry/SPR studies.
(18) For example, POP−Y could catch a photon, undergo charge separation ($POP^{+\bullet}$−$Y^{-\bullet}$), and transfer h^+ from $POP^{+\bullet}$ to TEOA (POP−$Y^{-\bullet}$). The electron would combine with the photogenerated $OPE^{+\bullet}$ at the domain interface to give OPE−$R^{-\bullet}$, which can transfer an e^- to Au (Figure S7). Thickness independence occurs because $Y^{-\bullet} \rightarrow OPE^{+\bullet}$ is limited to the domain interface. Direct photoreduction of R or OPE by $Y^{-\bullet}$ is less likely because $OPE^{+\bullet}$−$R^{-\bullet}$ forms in femtoseconds.[12]

JA101944R